Kinetics and Mechanism of β-Brass Dealloying in Aqueous 0.5 M Sodium Chloride Solution Derived from Combined Scanning Tunneling Microscopy and Electrochemical Data

J. Morales, P. Esparza, and S. Gonzalez

Departamento de Química Física, Universidad de La Laguna, Tenerife, Spain

L. Vazquez

Instituto de Ciencia de Materiales, CSIC, Departamento de Física Aplicada, C-XII, Universidad Autónoma de Madrid (UAM), 28049 Madrid, Spain

R. C. Salvarezza and A. J. Arvia*

Instituto de Investigaciones Fisicoquímicas Teóricas y Aplicadas (INIFTA), Sucursal 4, Casilla de Correo 16, 1900 La Plata, Argentina

Scanning tunneling microscopy (STM) combined with conventional electrochemical techniques was used to determine the kinetics and mechanism of β-brass dealloying in aqueous neutral solutions containing NaCl. In the potential range where selective dissolution of Zn occurs, electrochemical data suggest that the corrosion process is controlled by surface diffusion of Cu atoms. STM imaging of β-brass after dealloying shows the development of an irregular surface which attains a stationary regime. The irregular surface topography consists of faceted islands with atomically smooth terraces. For a constant dealloying time, the extent of faceting increases as the potential is moved positively, and at a constant applied potential it increases with electrodissolution time. The proportionality $\xi \propto L^\alpha$ was established, where ξ is the interface width related to L, the sample size. The exponent α is related to the degree of surface disorder. The value of α derived from STM is in the range $0.7 \leq \alpha \leq 0.8$, i.e. close to the predictions of aggregation models including surface diffusion.

1. Introduction

The stability of binary alloys in aqueous environments[1−4] depends on the alloy composition at the surface,[5] the solution composition,[6] the surface alloy pretreatment, and temperature.[7,8]

Dealloying appears as a complex process related to different problems such as metallic corrosion, including stress corrosion cracking, and heterogeneus catalysis. The loss of the alloy properties often occurs by dealloying, i.e., the selective dissolution of the less noble metal. In general, polarization curves for binary alloys in an agressive aqueous environment exhibit a region of very low potential-independent current (region a) followed by another region of a rapidly increasing current (region b). The potential transition between regions a and b takes place at E_c, the critical potential of the alloy. Below E_c, the electrodissolution of the most active species results in a protective metal layer of the most noble constituent which in turn, under favorable conditions, hinders the corrosion process. At this stage no remarkable changes in the corroding surface roughness can be observed. Conversely, above

E_c, the protective layer breaks, leading to massive dealloying and profuse surface roughening.

For Zn−Cu alloys (brass) immersed in aqueous NaCl solution, the transition from region a to region b cannot be determined because Cu begins to dissolve below E_c.[2] However, the selective dissolution in region a is easily achieved provided that E, the applied potential, is lower than the potential associated with the onset of Cu electrodissolution.

Several mechanisms have been proposed to explain dealloying. One of them, known as the divacancy mechanism,[9] considers that the electrodissolution rate of the less noble element is controlled by its solid state diffusion via divacancy formation.[10] Accordingly, the interface develops irregularities growing with time. Another mechanism for dealloying[11] considers that the surface diffusion of the most noble metal atoms is rate determining, leading to aggregates of the most noble element which finally produce an island−channel microstructure.

On the other hand, recent STM imaging on Au-rich Ag−Au alloy surfaces has shown that the electrodissolution proceeds from terraces forming cluster vacancies.[12] STM images taken during Cu electrodissolution from polycrystalline Cu_3Au[13] reveal the formation of two- (2D) and three-dimensional (3D) nuclei. In any case, independent of the mechanistic interpretation of dealloying, it is clear that this process is accompanied by a progressive rough-

[⊗] Abstract published in *Advance ACS Abstracts,* November 15, 1995.

(1) Kaiser, H. *Corrosion Mechanisms*; Mansfeld, F., Ed.; Marcel Dekker: New York, 1987; Chapter 23, p 85.

(2) Newman, R. C.; Shahrabi, T.; Sieradzki, K. *Corros. Sci.* **1988**, *28,* 873.

(3) Scully, J. C. *Met. Sci.* **1978**, *12*, 290 and references therein.

(4) Hardie, D.; Ebtehaj, K. *Br. Corros. J.* **1987**, *22*, 202.

(5) Pickering, H. W. *Corros. Sci.* **1983**, *23*, 1107.

(6) Moffat, T. P.; Fan, R. F.; Bard, A. *J. Electrochem. Soc.* **1991**, *138*, 3224.

(7) Trethewey, K.; Chamberlain, J. *Corrosion*; Longman: Essex, 1988, and references therein.

(8) Askeland, D. R. *The Science and Engineering of Materials*; PWS-Kent Publishing Company: Boston, MA, 1989.

(9) Pickering, H. W.; Wagner, C. *J. Electrochem. Soc.* **1967**, *114*, 698.

(10) Fritz, J. D.; Pickering, H. W. *J. Electrochem. Soc.* **1991**, *138*, 3209.

(11) Tischer, R. P.; Gerischer, H. *Z. Electrochem.* **1958**, *62*, 50. Forty, A. J.; Durkin, P. *Philos. Mag.* **1985**, *42*, 295. Sieradzki, K.; Corderman, R. R.; Shukla, K.; Newman, R. C. *Philos. Mag.* **1989**, *59*, 713.

(12) Oppenheim, I. C.; Trevor, D. J.; Chidsey, C. E. D.; Trevor, P. L.; Sieradzki, K. *Science* **1991**, *254*, 687.

(13) Burstein, G. T.; Gao, G. *J. Electrochem. Soc.* **1994**, *141*, 912.

ening of the dissolving interface.[14] However, despite the relevance of roughness development during dealloying, no quantitative data on the roughness characteristics of these systems have been reported so far.

In this paper the electrochemical behavior of β-brass is studied using potentiostatic and potentiodynamic techniques combined with "ex-situ" STM imaging. The roughness properties of β-brass, after dealloying at different potentials in region a, are interpreted by the dynamic scaling theory[15] applied to STM images. Results show that under different experimental conditions the value of α, the characteristic roughness exponent of the corroding specimen, is close to the predictions of aggregation models incorporating surface diffusion.

2. Experimental Section

Working electrodes (specimens) were made from β-brass bars, with the following chemical composition: 52.46% Cu, 47.49% Zn, 0.026% C, 0.005% Al, 0.023% Sn, As and Si < 0.001. Brass bars were made from known amounts of 99.999% Cu and 99.999% Zn by casting and melting. Drawn brass bars 0.6 cm in diameter were machined to obtain cylindrical specimens 0.3 cm in diameter. The base of the brass cylinder was used as a horizontal disk working electrode in contact with a hanging electrolyte solution column.[16] The working electrode (specimen) was wet-polished using different grain size emery papers, and finishing was made with 1 μm grit alumina paste. Then each specimen was successively rinsed with distilled acetone in an ultrasonic bath and with twice distilled water and, finally, dried in air at room temperature. Finally, specimens were lodged under low Ar pressure in a Pyrex tubing to be treated at 150 °C for 2 h to eliminate residual mechanical stresses and to improve their surface homogeneity. This pretreatment assured the reproducibility of results. After etching pretreated specimens in acid Fe₃Cl, a grain size density close to 50 grains cm⁻² was found, i.e., the alloy was formed by large grains so that a $1 \times 1 \mu$m² STM imaging was adequate to characterize a single grain surface. The $1 \times 1 \mu$m² STM image (Figure 1a) of the noncorroded specimen shows a relatively smooth topography (Figure 1b) with a root mean square roughness (ξ_{stm}) value close to 1.9 nm.[17]

Electrochemical runs were made using a conventional three-electrode Pyrex glass cell containing aqueous 0.5 M NaCl pH 7, at 25 °C, saturated with Ar. The potential of each specimen was measured against a saturated calomel electrode (SCE) provided with a conventional Luggin-Haber capillary tip arrangement. A large platinum wire was used as counterelectrode. All electrochemical runs were made at 25 °C.

Anodic polarization curves were run from −1.3 V in the positive potential direction at the scan rate $v = 2 \times 10^{-3}$ V s⁻¹. Voltammograms were also recorded in the range 0.05 V s⁻¹ < v < 0.2 V s⁻¹. Potentiostatic current transients were made by stepping E, the applied potential, from $E = -1.3$ V to an E_s value in the range −0.65 V < E_s < −0.45 V. Occasionally, the rotation speed of the working electrode was varied in the range $0 \leq \omega \leq$ 3000 rpm. In all cases the current density (j) was referred to the geometric area of the working electrode. During each run β-brass specimens were removed from the cell at a definite time (t), rinsed with twice-distilled Ar saturated water, dried under N₂, and finally kept under vacuum until proceeding to the ex-situ STM observation which typically takes no more than 4 h. The STM imaging was made using a Nanoscope III (Digital Instruments, Santa Barbara CA), Pt−Ir Nanotips, a bias voltage in the range 0.1 to −2.5 V at 1−5 nA constant current. To discard occasional imaging artifacts due to tip geometry, different tips were used, although no influence of the tip shape on our experimental data was detected. In order to minimize errors,[18] STM images with
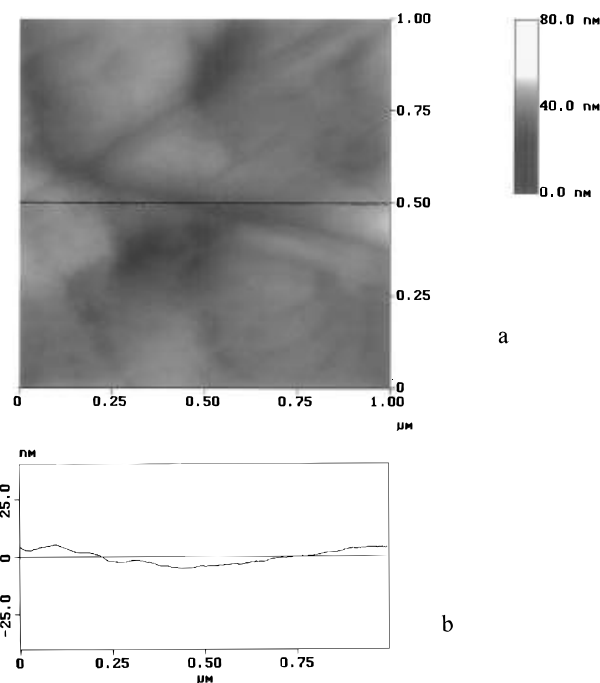
(14) Sieradzki, K. *J. Electrochem. Soc.* **1993**, *140*, 2868 and references therein.

(15) Family, F. *Physica A* **1990**, *168*, 561 and references therein.

(16) Elsner, C. I.; Schilardi, P.; Marchiano, S. L. *J. Appl. Electrochem.* **1993**, *23*, 1181.

(17) Shreir, L. L.; Jarman, R. A.; Burstein, G. T. *Corrosion*; Butterworth-Heineman Ltd: Oxford, 1994.

(18) Vázquez, L.; Salvarezza, R. C.; Herrasti, P.; Ocón, P.; Vara, J. M.; Arvia, A. J. *Appl. Surf. Sci.* **1993**, *70*, 413.

Figure 1. (a) A $1 \times 1 \mu$m² STM image of a noncorroded β-brass specimen (ξ_{stm} = 1.9 nm). (b) The cross section corresponds to the line marked in Figure 1a. A grain boundary is shown in the image.

512×512 pixels were taken. STM data were analyzed after fitting and removing the plane of the substrate.[19]

3. Results

3.1. Polarization Curves. Anodic apparent current density (j) vs potential (E) curves were recorded between −1.2 and −0.30 V at $v = 2 \times 10^{-3}$ V s⁻¹ in aqueous NaCl-containing solution (Figure 2a). These curves exhibit a cathodic current contribution related to the hydrogen evolution reaction (HER), followed by the broad anodic current peak A(I) at −0.80 V, a current plateau extending between −0.70 and −0.35 V and the small anodic peak A(II) in the range −0.48 < E < −0.40 V which largely overlaps the current plateau. Finally, for E > −0.4 V, a considerable increase in the anodic current (A(III)) was produced.

Both A(I) and A(II) and the anodic current plateau remained insensitive to the electrode rotation (ω) in the range 0 < ω < 2000 rpm.

3.2. Voltammetric Data. Voltammograms (first scan) run in aqueous NaCl-containing solution between −1.5 and −0.25 V at $v = 0.02$ V s⁻¹ (Figure 2b) show that peak A(I) consists of two anodic peaks, namely peak A(I)′ at −1.2 V and peak A(I)″ at −0.75 V. A slight increase in current related to peak A(II) is also observed at −0.5 V. The reverse scan shows peaks C(II) at −0.5 V, C(I)″ at −1.0 V, and C(I)′ at −1.2 V which are the conjugated peaks of A(II), A(I)′, and A(I), respectively, as concluded from those experiments in which the anodic and cathodic switching potentials were systematically changed. Likewise, the pairs of peaks A(II)/C(II) and A(III)/C(III) are clearly resolved when the cathodic switching potential is increased from −1.5 to −1.3 V (Figure 2c). Continuous cycling of the the brass electrodes produces a gradual change in the height of current peaks due to the increase in the surface area caused by the selective dissolution and accumulation of corrosion products. For this reason

(19) Krim, J.; Hevaert, I.; Haesendock, C.; Bruynseraede, Y. *Phys. Rev. Lett.* **1993**, *70*, 57.
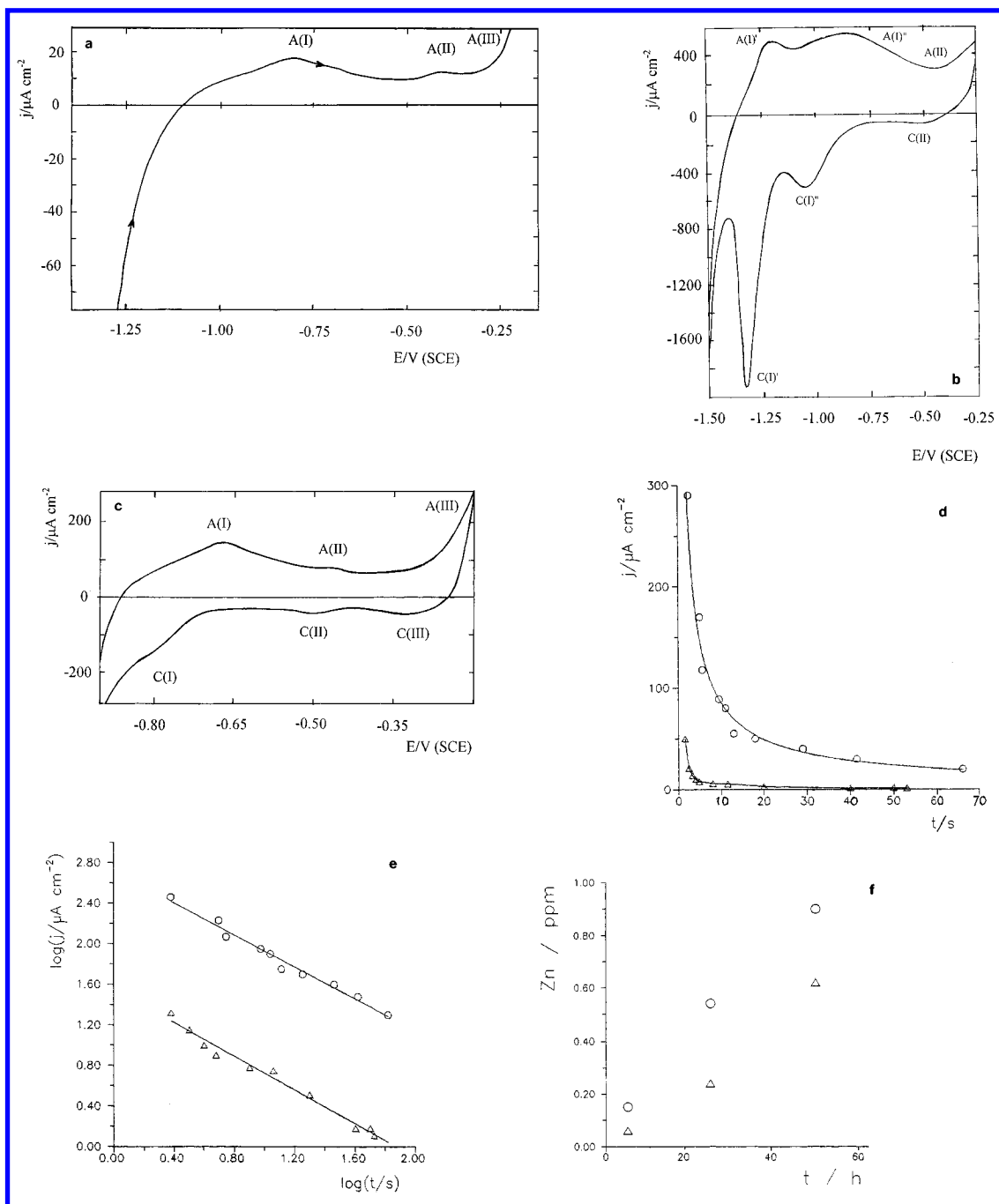
Figure 2. Electrochemical data resulting from β-brass immersed in aqueous 0.5 M NaCl, pH 7.0, 25 °C, $\omega = 0$ rpm: (a) anodic j vs E profile run between -1.3 and -0.3 V at $v = 2 \times 10^{-3}$ V s^{-1}; (b) voltammogram run between -1.5 and -0.25 V at $v = 0.02$ V s^{-1}; (c) voltammogram run between -1.3 and -0.25 V at $v = 0.02$ V s^{-1}, only the voltammogram from $E = -0.96$ V upward is shown; (d) anodic current decay at $E_s = -0.45$ V (○) and $E_s = -0.65$ V (△); (e) log j vs log t plots for anodic current transients shown in part d for $E_s = -0.45$ V (○) and $E_s = -0.65$ V (△); (f) amount of dissolved Zn (in ppm) vs t plots at $E_s = -0.625$ V (△) and $E_s = -0.45$ V (○).

only data from the first and second voltammetric scans were considered.

3.3. Potentiostatic Current Transients. The j vs t plots (Figure 2d) in aqueous NaCl-containing solution were recorded by stepping the potential from $E = -1.3$ V to an E_s value in the range -0.65 V $< E_s < -0.45$ V, which corresponds to the anodic current plateau in the polarization curves. These current transients fit a j vs $t^{-0.75}$ relationship for 0 s $\leq t \leq 100$ s (Figure 2e), in agreement with previously reported data on brass dealloying.[13] For $t > 200$ s a stationary anodic current density close to $3.0 \pm 0.5\,\mu$A cm^{-2} is attained. This constant current increases slightly with E_s, and it is independent of ω in the range $0 < \omega < 2000$ rpm.

3.4. Dissolution Products. The amount of Zn detected by atomic absorption spectroscopy in the aqueous NaCl-containing solution depends on E_s and t (Figure 2f). At a constant E_s, the Zn content in the solution increases linearly with t, whereas at a constant t, it increases as E_s is shifted from -0.625 to -0.45 V. In this potential range no soluble Cu can be detected by atomic absorption spectroscopy, in agreement with rotating ring–disk electrode data on Cu electrodissolution in aqueous 0.3 M NaCl.[20] Only when $E_s > -0.40$ V can the formation of soluble Cu(I) species be detected, i.e. when E_s lies in the

(20) Elsner, C.; Salvarezza, R. C.; Arvia, A. J. *Electrochim. Acta* **1988**, *33*, 1735.

potential range of peaks A(III)/C(III). Therefore, the anodic current plateau in the polarization curve definitely corresponds to the selective dissolution of Zn from the alloy with no Cu corrosion.

The amount of soluble Zn after 24 h correlates closely with the anodic charge involved in the potentiostatic current transients for the same period of time.

3.5. STM Imaging. The STM images of a β-brass grain kept for 24 h at $E_s = -0.625$ V (Figure 3a) differ markedly from the image of the untreated specimen (Figure 1). In fact, the STM image shown in Figure 3a corresponds to a β-brass specimen after a charge equivalent to the removal of 300 monolayers of pure Zn has been passed. This figure corresponds roughly to 600 monolayers of β-brass alloy. STM images (Figure 3a) of electrochemically treated specimens show islands following well-defined directions which intercept forming predominantly 30°, 60°, and 120° angles. A cross section of this topography (Figure 3b) shows islands 100−200 nm in average size and an island corrugation in the range 10−15 nm. The slope mode of the STM image at a high resolution reveals sawtooth steps (Figure 3c). At a higher magnification (Figure 3d−e), each island surface topography consists of an array of voids and clusters 10×20 nm^2 in average size. The surface of clusters is smooth as its corrugation is in the range 0.4− 1.0 nm. Voids 0.5−3 nm in depth are presumably formed by aggregation of vacancies resulting from dealloying.[21] Otherwise, after a 48 h polarization at $E = -0.625$ V the island structure smears out, and then 3D clusters and facets tend to dominate the entire topography (Figure 3f,g).

On the other hand, the STM image of a β-brass specimen held at $E_s = -0.45$ V for 24 h, i.e., at a potential at which Cl$^-$-ion electroadsorption takes place (peak A(II)), shows again the aforementioned island−void structure, but the surface at islands is fully faceted (Figure 4a). The cross section (Figure 4b) derived from this image exhibits islands 200 nm or thereabouts in size, and a 7−10-nm surface corrugation. Each island comprises a number of regular facets aligned in a well-defined direction (Figure 4c). STM images at a higher magnification reveal terraces and sawtooth steps (Figure 4d). The cross section (Figure 4e) shows that terraces are atomically smooth and that some steps are monoatomic in height. Those domains 10 nm^2 in size (Figure 4f) forming smooth terraces probably result from the coalescence and relaxation of clusters similar to those depicted in Figure 3d,e. Therefore, the presence of atomically smooth terraces resulting from dealloying at $E_s = -0.45$ V may involve a faster vacancy aggregation than that at $E_s = -0.65$ V. This conclusion, is consistent with the enhanced Cu surface atom mobility caused by Cl$^-$-ion electroadsorption at $E_s = -0.45$ V.[22] Similar surface patterns can be observed for β-brass specimens held at $E_s = -0.45$ V for $t = 50$ h.

It should be noted that in the analysis of the STM images of β-brass, image quality is improved by using a tip−sample voltage in the range −0.5 to −1.0 V, a working condition which points out the likely presence of a thin ZnO or CuCl coating formed in region a. Hence, the atomic corrugation observed at smooth surfaces yielding the interatomic distance $d \cong 0.4$ nm, and a corrugation close to 0.2 nm in height (Figure 4f), could be assigned to either a ZnO or CuCl thin layer on the specimen. In fact, recent STM data reported for Cu electrodissolution in aqueous NaCl solution have yielded similar values of d which has been assigned to a CuCl layer.[22]

(21) Chen, S. J.; Sanz, F.; Ogletree, D. F.; Hallmark, V. M.; Devine, T. M.; Salmeron, M. *Progress in the Understanding and Prevention of Corrosion*; Costa, J. M., Mercer, A. D., Eds.; The Institute of Materials: London, 1993; p 1664.

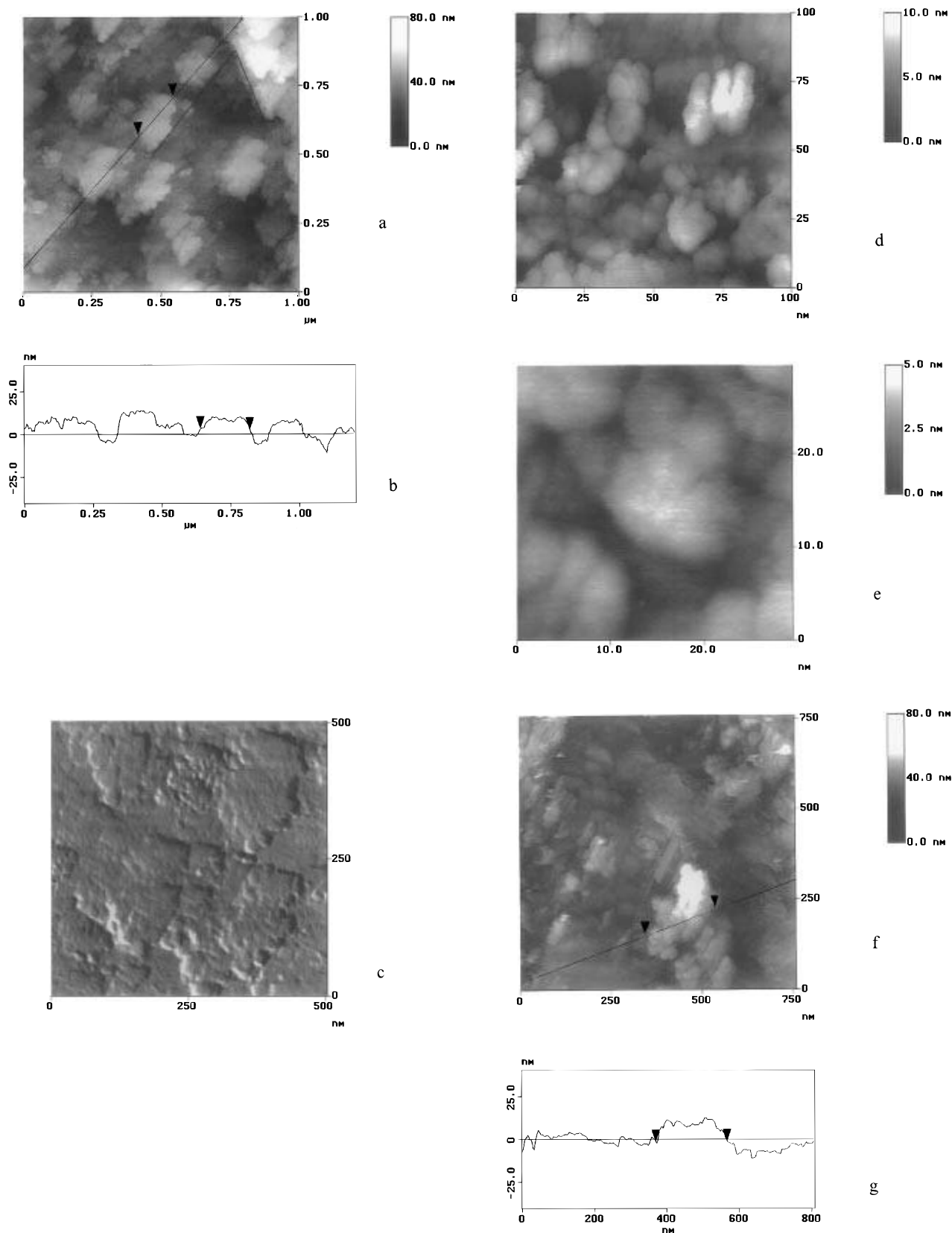(22) Suggs, D. W.; Bard, A. J. *J. Am. Chem. Soc.* **1994**, *116*, 10725.

For $1 \times 1\ \mu$m^2 STM images of β-brass held at $E_s = -0.45$ V in the aqueous NaCl-containing solution, the root mean square roughness (ξ_{stm}) seems to increase with electrodissolution time until a constant ξ_{stm} value for $t > 20$ h is attained (Figure 5). On the other hand, ξ_{stm} values resulting from STM images of specimens held at $E_s = -0.625$ V are smaller than those obtained for $E_s = -0.45$ V in the same solution, although a constant value is also attained. This difference in values of ξ_{stm} is consistent with an increasing dealloying as E_s is shifted positively (Figure 2f). Therefore, from the analysis of data shown in Figures 2f and 5, it can be concluded that for a constant rate of dealloying a steady-state regime for the width of the reacting interface is reached. This means that the value of the root mean square roughness remains unchanged with dealloying time.

4. Discussion

4.1. Processes Involved in β-Brass Electrodissolution in Aqueous NaCl Containing Solution. The electrochemical dissolution of β-brass in an aqueous solution containing NaCl involves a number of conjugated processes occurring at well-defined potential regions. Anodic peaks A(I)′ and A(I)″ are related to the electroformation of a ZnO·xH$_2$O layer, and Zn electrodissolution leading to a depletion of Zn atoms at the alloy surface and the formation of a Cu-rich layer.[2,13] As the conjugated cathodic peaks C(I)′ and C(II)″ involve only a 1.2 mC cm^{-2} apparent charge density, the thickness of the ZnO layer should not exceed two to three monolayers as 0.4 mC cm^{-2} $\cong$ 1 monolayer of ZnO.

The anodic current plateau is related to the dealloying of β-brass as in this potential range soluble Zn, probably ZnCl$_4^{2-}$, and no soluble Cu species are found. Hence, according to these results the anodic current plateau should be mainly related to dealloying involving the preferential electrodissolution of Zn through a thin, and presumably incomplete, ZnO·xH$_2$O layer. The fact that the current plateau is independent of ω allows us to discard a dealloying kinetics controlled by the diffusion of ZnCl$_4^{2-}$ ions from the metal surface outward.

On the other hand, the small and reversible A(II)/ C(II) conjugated pair of peaks (Figure 2a−c) is assigned to the electroadsorption of Cl$^-$ on the Cu-rich areas.[19] Finally, the marked increase in current related to peak A(III) can be attributed to the electrodissolution of both Cu and Zn as ZnCl$_4^{2-}$ and CuCl$_2^-$ complexes, respectively, and CuCl electroformation,[20] whereas peak C(III) can be assigned to the electroreduction of soluble Cu species[20] produced in the preceding anodic potential scan.

4.2. The Probable Reaction Mechanism of β-Brass Dealloying. Dealloying of β-brass can be described as a localized corrosion process at the atomic level which seemingly occurs at a stirring-independent and slightly-dependent potential rate. These kinetic characteristics would imply a rate-controlling step involving either a diffusion of Zn atoms from bulk alloy to the corroding surface or a surface diffusion of the remaining Cu atoms. The first possibility corresponds to a solid state diffusion mechanism[9] which at a constant E_s predicts a $j \propto t^{-1/2}$ relationship for $t \rightarrow 0$, rather than the $j \propto t^{-0.75}$ dependence experimentally observed. Therefore, the first explanation should be, in principle, ruled out. In fact, the $j \propto t^{-0.75}$ decay law can be related to a dealloying mechanism involving a surface diffusion process with presumably Cu atoms as rate controlling.[13]

Further arguments in favor of a dominant contribution of Cu atom surface mobility to the kinetics of β-brass dealloying can be derived from the topographic analysis

Figure 3. STM images of a β-brass specimen after polarization at $E_s = -0.625$ V in aqueous 0.5 M NaCl for the time t, 25 °C, $\omega = 0$ rpm: (a) a 1×1 μm^2 STM image, $t = 24$ h, the marked angle is 60°; (b) cross section at the line marked in Figure 3a, island profiles are resolved, a 190 nm island size is marked by arrows; (c) a 500×500 nm^2 STM image (slope mode), $t = 24$ h, island borders can be distinguished; (d) a 100×100 nm^2 3D STM image, $t = 24$ h; (e) a 30×30 nm^2 3D STM image, $t = 24$ h; (f) a 750 $\times$ 750 nm^2 STM image, $t = 48$ h; (g) cross section at the line marked in Figure 3f, the size of the 200 nm remaining island is marked by arrows.

of the corroding interface itself. Experimental data show that as E_s is moved to the potential range of peak A(II), the surface coverage by Cl$^-$ increases, and accordingly, smoother terraces are formed. Under these conditions, however, the value of ξ_{stm} increases due to the faceting produced as E_s is shifted positively (Figure 5).
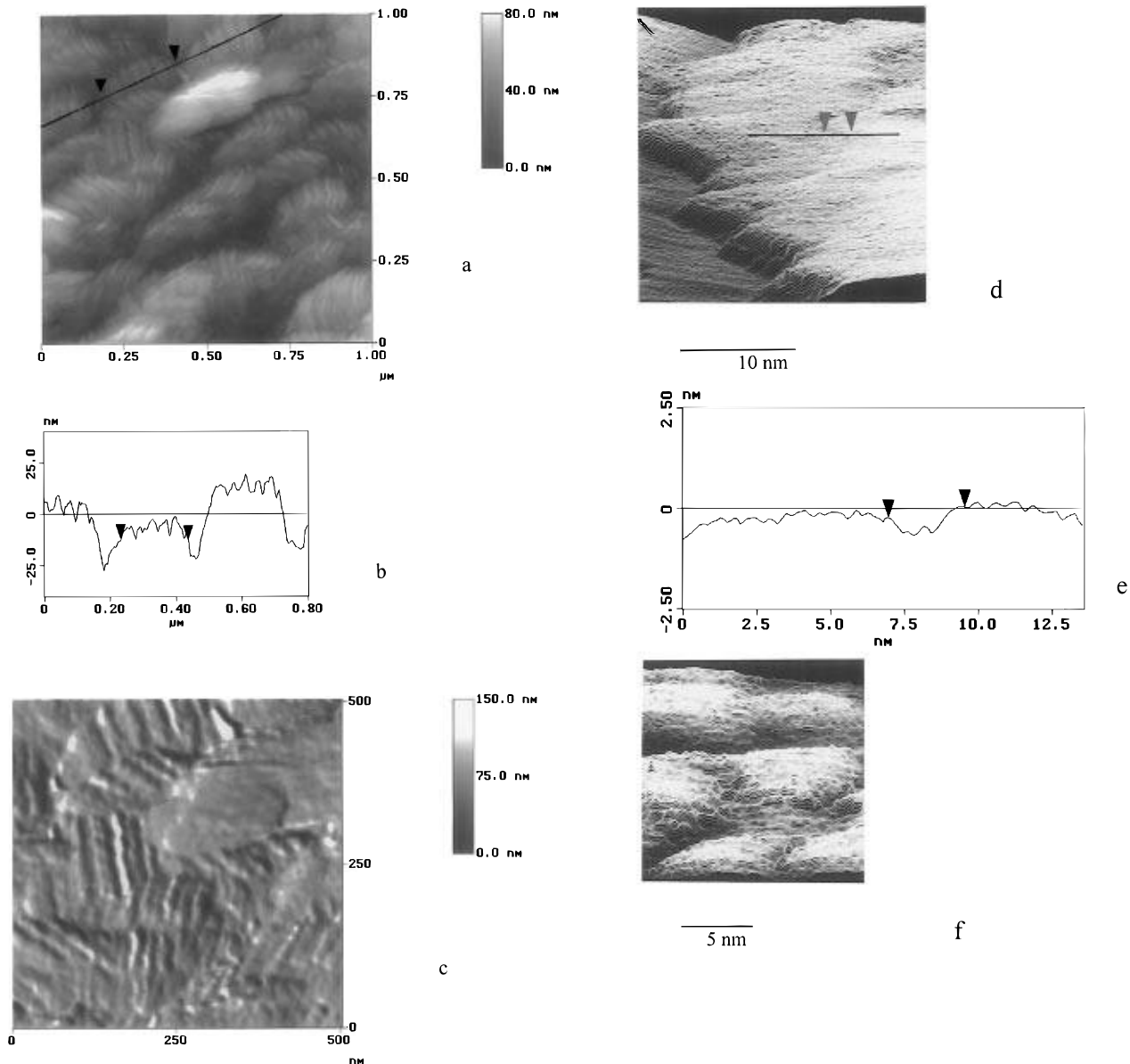
Figure 4. STM images of a β-brass specimen after polarization at $E_s = -0.450$ V in aqueous 0.5 M NaCl for the time $t = 24$ h, 25 °C, $\omega = 0$ rpm: (a) a 1×1 μm^2 STM image; (b) cross section taken as indicated by the line marked in Figure 4a, island profiles are resolved, a 200 nm island size is marked by arrows; (c) a 500×500 nm^2 STM image (slope mode), faceted islands can be distinguished; (d) a 25×25 nm^2 3D STM image, height difference $0 \leq z \leq 3$ nm; (e) cross section taken as indicated by the line marked in Figure 4d, atomically smooth terraces and monoatomic height steps are shown, arrows indicate a 0.27 nm vertical distance; (f) a 15×15 nm^2 3D STM image, height difference $0 \leq z \leq 2$ nm.

The roughness evolution of the corroding interface can be analyzed in terms of the dynamic scaling theory.[15] This theory predicts that $\xi(L,\langle h \rangle)$, the root mean square roughness for a sample formed by N particles, length L, and average thickness or height $\langle h \rangle$, scales as

$$\xi(L,\langle h \rangle) \propto L^\alpha \, f(x) \tag{1}$$

where $\xi(L,\langle h \rangle)$ is defined by

$$\xi(L,\langle h \rangle) = [1/N\sum[h(x_i) - \langle h \rangle]^2]^{1/2} \tag{2}$$

$h(x_i)$ is the deposit height measured along the x-direction at the point x_i, and $x = \langle h \rangle/L^{\alpha/\beta}$. Furthermore, $f(x)$ has the following properties: $f(x) = $ const for $x \Rightarrow \infty$, and $f(x) = x^\beta$ for $x \Rightarrow 0$. Therefore, for $\langle h \rangle \Rightarrow 0$ eq 1 becomes

$$\xi(\langle h \rangle) \propto \langle h \rangle^\beta \tag{3}$$

whereas for $\langle h \rangle \Rightarrow \infty$, $\xi(L,\langle h \rangle)$ reaches a steady state, and

eq 1 becomes

$$\xi(L) \propto L^\alpha \tag{4}$$

where β and α are the dynamic and static growth exponents, respectively.

The value of α is related to D_s, the local fractal dimension, of the self-affine surface through the relationship

$$D_s = d - \alpha \tag{5}$$

where d is the space dimension of the corroding interface. Accordingly, the value of α contains valuable information about the corroding surface disorder and the mechanism of the rough interface growth.[15] To evaluate α, it is necessary that the steady state roughness regime be attained. Experimental data (Figure 5) indicate that this roughness is attained for β-brass polarized for 24 h at either $E_s = -0.625$ V or $E_s = -0.45$ V. Then, the value
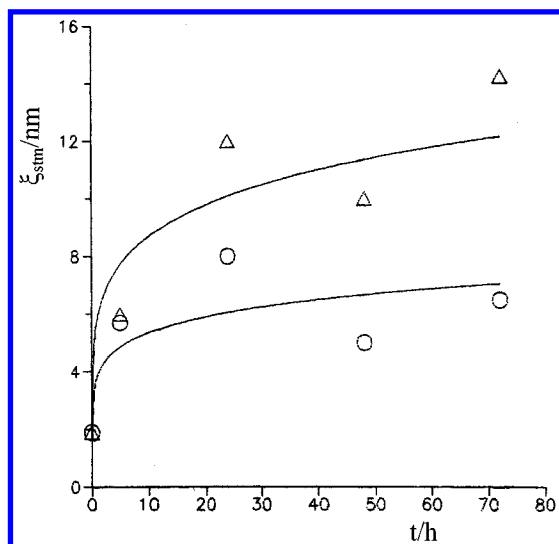
Figure 5. ξ_{stm} vs t plots derived from $1 \times 1 \ \mu m^2$ STM images of β-brass after polarization in aqueous 0.5 NaCl at $E_s = -0.625$ V ($\bigcirc$) and $E_s = -0.45$ V ($\triangle$), 25 °C.

of α can be obtained from the analysis of STM images by using the single image dynamic scaling method.[18,23]

The single image dynamic scaling derives the value of α from the equation

$$\xi_{stm}(L_s,\langle h \rangle) \propto L_s{}^{\alpha} \qquad (6)$$

by plotting log ξ_{stm} vs log L_s, where L_s is the length of a segment of the STM scan of size S measured in the x-direction. For each scan, 486 pairs of data points (L_s, ξ_{stm}) have been obtained, L_s being varied from $S/128$ to $0.96S$. Finally, for each L_s, the corresponding ξ_{stm} represents the average value resulting from 512 scans of the same image.

The log ξ_{stm} vs log L_s plots (Figure 6a) resulting from STM images of β-brass surfaces polarized for 24 h at $E_s = -0.65$ V approach a straight line with the slope of 0.67 $\pm$ 0.05 covering more than 1 decade in L_s. On the other hand, the log ξ_{stm} vs log L_s plots (Figure 6b) resulting from STM images of β-brass polarized for 24 h at $E_s = -0.45$ V also result in straight lines with the slope $\alpha = 0.80 \pm 0.07$ for more than 2 decades of magnitude in L_s and a saturation region for $L_s > 200$ nm. This value of L_s is close to the average size of islands observed by STM imaging. Furthermore, straight line plots presented in Figure 6 are displaced upward, i.e., to larger ξ_{stm} values, as E_s is displaced positively.

It should be noted that for computer-simulated fractals, data covering 4 to 5 orders of magnitude are required for logarithmic fitting. However, for experimental systems this goal is less ambitious due to the existence of inner and outer cutoffs.[15] This means that the fractal character of a real system is restricted to well-defined limits. For our system the inner cutoff should be related to the size of atoms and the outer cutoff to the size the islands. Obviously, in $1 \times 1 \ \mu m^2$ STM images used for fractal characterization only the outer cutoff can be clearly determined. Accordingly, the log ξ_{stm} vs log L_s linear plots derived from experimental data covering approximately at least 1 order of magnitude are considered acceptable.

Average values of α resulting from 15 different STM images taken in the range 25 nm $< L_s <$ 1000 nm, for β-brass surfaces polarized at either $E_s = -0.45$ V or $E_s = -0.65$ V, are $\langle \alpha \rangle = 0.80 \pm 0.07$ and $\langle \alpha \rangle = 0.70 \pm 0.05$,
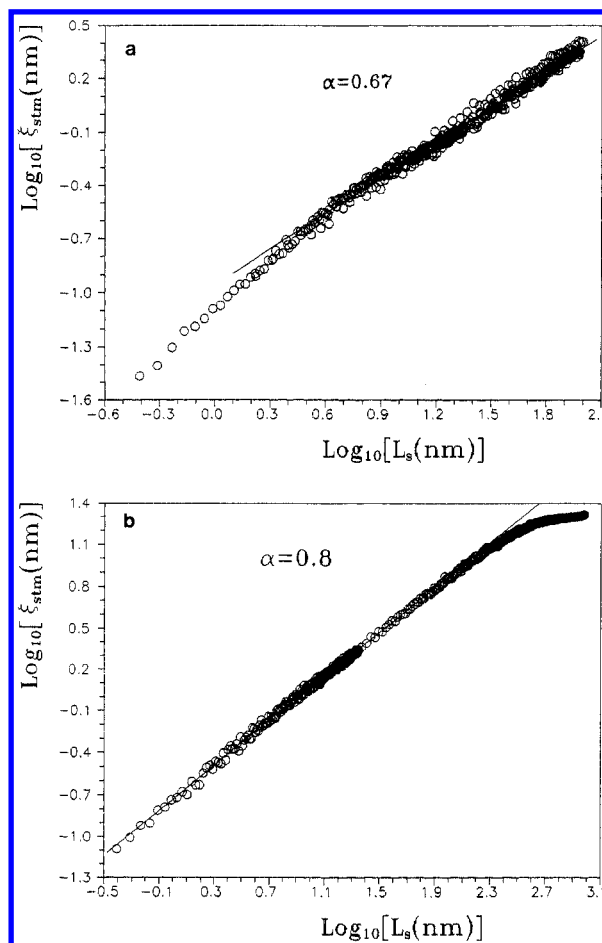
(23) Vázquez, L.; Salvarezza, R. C.; Herrasti, P.; Ocón, P.; Vara, J. M.; Arvia, A. J. *Chaos, Solitons and Fractals* **1995**, *6*, 569.

Figure 6. log ξ_{stm} vs log L_s plot resulting from STM images of β-brass polarized in aqueous 0.5 M NaCl at $E_s = -0.625$ V (a) and $E_s = -0.45$ V (b), 25 °C. Data correspond to the steady state roughness regime at the dissolving interface ($t = 24$ h, see Figure 5).

respectively. Similar values of α were obtained for β-brass specimens kept at either $E_s = -0.625$ V or $E_s = -0.45$ V for 72 h. The increase in the value of α from 0.70 to 0.80 indicates the dominant influence of faceting on the topography of the corroding interface as E_s is increased positively. It should be noted that $\alpha = 1$ is expected for an ideal stepped surface with smooth terraces.[24]

The value of α provides information about the probable interface growth mechanism. Several growth models, such as the Eden,[25] ballistic deposition,[26] and restricted solid-on-solid models,[27] have been proposed to explain nonequilibrium interface growth processes. These models can be successfully described by the Kardar, Parisi, and Zhang motion equation[28] which leads to $\alpha = 0.4$ in 3D space. Alternate models in 3D space incorporating surface diffusion yield either $\alpha = 1.0$[29,30] or $\alpha = 0.66$.[31] Despite the fact that these models are related to the development of a rough interface by aggregation rather than removal

(24) Salvarezza, R. C.; Arvia, A. J. *Modern Aspects of Electrochemistry*, in press.
(25) Eden, M. *Proceeding of the 4th Berkeley Symposium on Mathematical Statics and Probability*; Neyman, F., Ed.; University of California Press: Berkeley, 1961; Vol. 4.
(26) Meakin, P.; Ramanlal, P.; Sander, L. M.; Ball, R. C. *Phys. Rev. A* **1986**, *34*, 509.
(27) Gilmer, G. H.; Bennema, P. *J. Appl. Phys.* **1992**, *43*, 1347.
(28) Kardar, M.; Parisi, G.; Zhang, Y. C. *Phys. Rev. Lett.* **1986**, *56*, 889.
(29) Wolf, D.; Villain, J. *Europhys. Lett.* **1990**, *13*, 389. Villain, J. *J. Phys. I* **1992**, *1*, 19.
(30) Siegert, M.; Plischke, M. *Phys. Rev. Lett.* **1994**, *73*, 1517.
(31) Lai, Z. W.; Das Sarma, S. *Phys. Rev. Lett.* **1991**, *66*, 2348.

of material, it is clear that the corroding β-brass surface can be considered as a self-affine fractal resulting from vacancy aggregation. The surface mobility of the remaining Cu atoms results in the coalescence of vacancies and surface clustering leading to the characteristic void−cluster rough topography.

The role of surface mobility in determining the topography of the corroding interface is supported by the experimental values of α which are between $\alpha = 1.0$[29,30] and $\alpha = 0.66$[31] predicted for the interface growth models with surface diffusion.

Therefore, these models appear to be adequate to describe the rough β-brass surface topography developed in the corrosion process in aqueous NaCl-containing solution at room temperature.

The preceding mechanistic conclusion is not surprising due to the high surface mobility of Cu in vacuum, air, and liquids at room temperature,[32] especially in contact with Cl⁻ in the environment.[33] The slight increase in β-brass electrodissolution with E_s should be related to an enhanced surface mobility of Cu atoms produced as the Cl⁻ surface coverage increases.[34]

Finally, it should be noted that the bulk diffusion of Zn becoming a rate-determining step in the kinetics of β-brass electrodissolution in aqueous environments would have led to a branched DLA-like interface[35] rather than the faceted island-like topography observed by STM imaging. Therefore, this observation, and the j vs $t^{-0.75}$ current decay law support a surface diffusion controlling mechanism for the kinetics of β-brass dealloying in aqueous NaCl-containing solution.

Conclusions

For the first time it has been demonstrated that a corroded surface of an alloy can be described as a self-affine fractal obeying the relationship $\xi \propto L^\alpha$ with α values compatible with a vacancy aggregation process with surface diffusion contributions. Therefore, the analysis of the rough topography under the steady state regime provides a new way to determine the mechanism of corrosion processes.

(32) Behm, R. J. *Scanning Tunneling Microscopy and Related Methods*; Behm, R. J., García, N., Röhrer, H., Eds.; Kluwer Academic Publishers: Boston, MA, 1989; p 173.

(33) Bonzel, H. P. *Surface Physics of Materials*; Blakely, J. M., Ed.; Academic Press: New York, 1975; p 280.
(34) García, P.; Goméz, M.; Salvarezza, R. C.; Arvia, A. J. *J. Electroanal. Chem.* **1993**, *347*, 237.
(35) Hernández-Creus, A.; Salvarezza, R. C.; Arvia, A. J. In preparation.